Optik 135 (2017) 57–69

Contents lists available at ScienceDirect

Optik

journal homepage: www.elsevier.de/ijleo

Original research article

Electronic structure and optical properties of dilute boron-bismide quaternary alloys $B_xGa_{1-x}As_{1-y}Bi_y$/GaAs for infrared optoelectronic devices

Abdenacer Assali [a,b,*], M'hamed Bouslama [b], A.H. Reshak [c,d], Samir Zerroug [e], Hamza Abid [f]

[a] Centre de Développement des Technologies Avancées, Unité de Recherche en Optique et Photonique, UROP – CDTA, Université Ferhat Abbas Sétif 1, 19000 Sétif, Algeria
[b] Laboratoire Matériaux (LABMAT), Ecole Nationale Polytechnique d'Oran (ENPO), BP 1523 El Mnaouar, 31000 Oran, Algeria
[c] New Technologies—Research Centre, University of West Bohemia, Univerzitni 8, 306 14 Pilsen, Czechia
[d] Center of Excellence Geopolymer and Green Technology, School of Material Engineering, University Malaysia Perlis, 01007 Kangar, Perlis, Malaysia
[e] Département des Troncs Communs, Faculté des Sciences de la Nature et de la Vie, Université Mira–Bejaia, Bejaia 6000, Algeria
[f] Laboratoire des Matériaux Appliqués, Centre de Recherche, Université de Sidi Bel Abbès, 22000 Sidi Bel Abbès, Algeria

ARTICLE INFO

Article history:
Received 28 August 2016
Received in revised form 26 October 2016
Accepted 24 January 2017

Keywords:
BGaAsBi/GaAs
Infrared optoelectronic devices
DFT theory
Electronic structure
Optical constants

ABSTRACT

Electronic structure and optical properties of the dilute boron-bismide quaternary $B_xGa_{1-x}As_{1-y}Bi_y$ alloys have been investigated from first-principles. The calculated structural parameters are found to be in excellent agreement with the experimental data. Optical properties are calculated by the recent developed Tran–Blaha-modified Becke–Johnson (TB-mBJ) potential which gives accurate band gaps. We find that incorporation of B and Bi into GaAs resulted in a reduced band gap. A quaternary $B_xGa_{1-x}As_{1-y}Bi_y$ alloy with $x = y = 0.125$ is predicted to be lattice-matched to GaAs. The optical properties of $B_xGa_{1-x}As_{1-y}Bi_y$ depend on the incorporated of B and Bi contents. This makes $B_xGa_{1-x}As_{1-y}Bi_y$/GaAs a promising system for the design of high-efficiency solar cells and advanced infrared Laser Diodes.

1. Introduction

Bismuth containing III–V alloys have attracted great attention because of their potential applications in long-wavelength emitters, detectors, semiconductor laser diodes, solar cells, and spintronics [1–4]. In particular, GaAsBi has been proposed as an alternative material to the conventional III-Nitrides such as GaAsN, interesting for optoelectronic devices and multijunction solar cells [5,6]. Incorporation of a few percent of Bi in GaAs leads to a strong reduction of the band gap (≈90 meV/%Bi) [7] without affecting the optical and transport properties.

Dilute GaAsBi has been grown by metal organic chemical vapor deposition (MOCVD) [8] and molecular beam epitaxy (MBE) [9]. The structural, electronic and optical properties of $GaAs_{1-x}Bi_x$ alloys have been studied using DFT calculations based on the FP-LAPW method [10–12].

* Corresponding author.
E-mail addresses: assali_nacer@yahoo.fr, aassali@cdta.dz (A. Assali).

http://dx.doi.org/10.1016/j.ijleo.2017.01.059
0030-4026/

However, higher Bi-content in GaAs leads to a significant increase in lattice parameter causing structural defects, such as dislocations at the interface layers, and degraded the performance of optoelectronic devices and reduces efficiency of solar cells [13].

One way to solve the lattice mismatch problem is to incorporate both N and Bi in GaAs to form GaAsNBi alloy as proposed by Janotti et al. [14].

In the present paper, we investigate the incorporation of Boron (B) into $GaAs_{1-x}Bi_x$ in the form of $B_yGa_{1-y}As_{1-x}Bi_x$ quaternary alloys as an alternative to GaAsNBi.

BGaAsBi alloy has been grown on GaAs substrates by Beaton et al. [15] using solid-source MBE method. Aslan et al. [16] studied the structural and electronic properties of BGaAsBi alloys using the full potential linearized augmented plane wave method within Wu-Cohen (WC-GGA) approach. Optical properties of BGaAsBi alloy are not studied yet.

Here we use density functional theory DFT and the FP-LAPW method to study the structural, electronic and optical properties of zinc blende $B_xGa_{1-x}As_{1-y}Bi_y$ alloys for different concentrations of B and Bi (0.062, 0.125 and 0.187). We first compute the ground state properties such as lattice parameter and bulk modulus for the binary zinc blende GaAs, BAs, GaBi and BBi and their ternary $GaAs_{1-x}Bi_x$, $B_yGa_{1-y}As$ and quaternary $B_xGa_{1-x}As_{1-y}Bi_y$ alloys matched to GaAs. Then, we have calculated the electronic structure and the density of states of alloys. Finally, we investigate the optical properties of zinc blende $B_xGa_{1-x}As_{1-y}Bi_y$ alloys for different Bi and B compositions, using the relaxed structural parameter of these alloys.

We find that BGaAsBi alloys have band gaps in the range of [0.683−1.678] eV corresponding to the wavelength range [0.73−1.81] μm, by varying the Bi and B contents, keeping their lattice-matched equal to that of GaAs and cover the optical fiber communication wavelength.

2. Methodology

To investigate the structural, electronic, and optical properties of the zinc blende binary GaAs, BAs, GaBi and BBi and their alloys $GaAs_{1-x}Bi_x$, $B_yGa_{1-y}As$ and $B_xGa_{1-x}As_{1-y}Bi_y$, we performed the full-potential linearized augmented plane wave (FP-LAPW) calculations within the framework of density functional theory (DFT) [17], as implemented in the WIEN2K code [18]. The exchange-correlation potential for structural properties was treated by the Wu-Cohen generalized gradient approximation (GGA-WC) [19]. For the electronic calculations, we used different schemes to describe the exchange-correlation potential, such as the Tran–Blaha-modified Becke–Johnson (TB-mBJ) potential [20], the Perdew-Burke-Ernzerhof generalized gradient approximation (GGA-PBE) [21] and GGA-WC approximations. The optical properties are computed using the TB-mBJ potential. The wave functions, charge density and potential inside the muffin-tin spheres are expanded with an angular momentum $l_{max} = 10$. In the interstitial regions, the wave functions are expanded in plane wave (PWs) with a cut-off of about $R_{MT}K_{max} = 7$, where R_{MT} is the smallest muffin-tin radius and K_{max} is the largest k vector in the plane wave's expansion. The B ($s^2\ 2p^1$), Ga ([Ar] $3d^{10}\ 4s^2\ 4p^3$), As ([Ar] $4d^{10}\ 5s^2\ 5p^1$) and Bi ([Xe] $4f^{14}\ 5d^{10}\ 6s^2\ 6p^3$) states are treated as valence electrons. The muffin-tin radius for B, Ga, As and Bi are taken as 1.65, 2.05, 2.06 and 2.32 a.u, respectively.

A 32-atom supercell is used for modeling the structure of the alloys, which corresponds to $2 \times 2 \times 1$ repetition of the conventional cubic unit cell. We have considered the zinc blende structure for all concerned materials used in this study, assuming that the alloys will be stable in the structure of the parent compound GaAs. All the atomic positions and lattice parameters were optimized. The integrations over the Brillouin-zone were performed using a Monkorst-Pack mesh [22] of 72 special k-points for the binary compounds, and 30 special k-points for ternary and quaternary alloys. Both of plane wave cut-off and the number of k-points were chosen in order to ensure convergence of total-energy differences.

Fig. 1 shows the supercell structures of $GaAs_{0.812}Bi_{0.187}$, $B_{0.187}Ga_{0.812}As$ and $B_{0.187}Ga_{0.812}As_{0.812}Bi_{0.187}$ alloys. Table 1 summarizes the geometrical arrangement of B and Bi atoms in the relaxed structure of $B_xGa_{1-x}As_{1-y}Bi_y$ alloys.

3. Results and discussion

3.1. Structural properties

A Binary parent compounds

We first discussed the structural properties of GaAs, BAs, GaBi and BBi compounds in the zinc blende structure. The structural parameters are obtained from the total energy calculations as a function of unit cell volume. This is performed by the scalar non-relativistic FP-LAPW method within the GGA-WC approximation. The obtained total-energy values are fitted to the Murnaghan's equation of state [23] to obtain the equilibrium structural parameters such as the lattice constant and bulk modulus.

The results are summarized in Table 2 and compared with available experimental data and previous theoretical works. The calculated structural parameters are very close to the experimental values, with an error of about 1.8% for GaAs, 0.7% for BAs, and 0.7% for GaBi. The GGA-WC scheme gives lattice constants in better agreement with experimental data than the standard GGA-PBE and the LDA approximations [24]. It is known that the GGA-PBE overestimates the lattice parameters, while LDA underestimates them [25,26]. The bulk modulus decreases when we move from GaAs → BAs and from BBi → GaBi, i.e., from

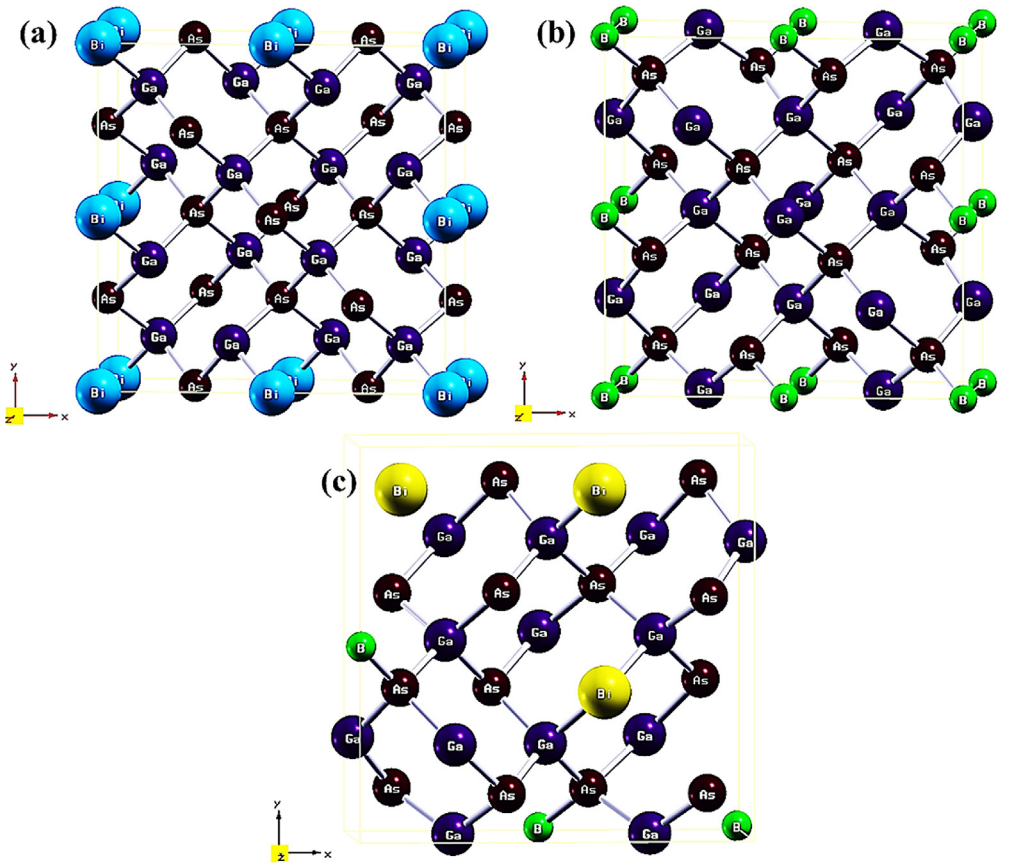

Fig. 1. Zinc blende relaxed structure for (a) $GaAs_{0.812}Bi_{0.187}$, (b) $B_{0.187}Ga_{0.812}As$ and (c) $B_{0.187}Ga_{0.812}As_{0.812}Bi_{0.187}$ ($2a \times 2b \times c$ supercell).

the lower atomic Z number to the higher one. This means that the GaBi is more compressible than the other compounds. The bulk modulus is related to the lattice constants within the reverse relation: $B \propto V_0^{-1}$, where V_0 is the unit cell volume.

B Ternary and quaternary $B_xGa_{1-x}As_{1-y}Bi_y$ alloys

We studied the effect of dilute B and Bi contents on the structural properties of zinc blende ternary $GaAs_{1-x}Bi_x$, $B_xGa_{1-x}As$ and quaternary $B_xGa_{1-x}As_{1-y}Bi_y$ alloys for x and y varying up to 0.187. Table 3 summarizes the computed properties of zinc blende $GaAs_{1-x}Bi_x$, $B_xGa_{1-x}As$ and $B_xGa_{1-x}As_{1-y}Bi_y$ alloys for different B and Bi contents compared to other theoretical data. Our results are found to be less than the ones reported by Aslan et al. [16]. It is noticeable that, no experimental data are found of the studied alloys for comparison.

Fig. 2 shows the variation of lattice constant as a function of B and Bi concentrations in $GaAs_{1-x}Bi_x$, $B_xGa_{1-x}As$ and $B_xGa_{1-x}As_{1-y}Bi_y$ alloys.

It is observed that the Bi-induced in $GaAs_{1-x}Bi_x$ leads to an increase of the lattice constant over a range of 12.1%, while the B-induced in $B_xGa_{1-x}As$ leads to a decrease of the lattice constant over a range of 17.1%. This is explained by the large atomic size of Bi than As and Ga than B. Thus, the incorporation of Bi in $GaAs_{1-x}Bi_x$ and B in $B_xGa_{1-x}As$ allow increasing mismatch with GaAs substrates leading to generate high misfit dislocations and strain in these heterostructures. Consequently, structural defects enhance nonradiative recombinations that responsible to limited luminescence efficiency in alloys [36].

A quadratic fit of the lattice constant of ternary alloys by a second-order polynomial, gives the following relations

$$\begin{cases} a_{GaAs_{1-x}Bi_x} = 5.6689 + 0.8544x - 0.64x^2 \\ a_{B_xGa_{1-x}As} = 5.6685 - 0.80808x - 0.0704x^2 \end{cases} \quad (1)$$

A slight deviation from linear Vegard's law is obtained, with $b = -0.0704$ Å for the relaxed $B_xGa_{1-x}As$ alloys. However, a large deviation of $b = -0.64$ Å is obtained for the relaxed $GaAs_{1-x}Bi_x$ alloys. This is explained by the relaxation effect of the Ga-As and Ga-Bi/B-As bond lengths. The bowing lattice parameter is due to the mismatch between the constituent binaries alloys, which increases with increasing mismatch.

Table 1
Atomic positions of B and Bi incorporated in the relaxed structure of $B_xGa_{1-x}As_{1-y}Bi_y$ alloys.

	Concentrations	B positions (*x*,*y*,*z*)	Bi positions (*x*,*y*,*z*)
$GaAs_{1-x}Bi_x$	0.062	–	Bi (0.0, 0.0, 0.0)
	0.125	–	Bi_1 (0.5, 0.0, 0.0)
			Bi_2 (0.0, 0.5, 0.0)
	0.187	–	Bi_1 (0.0, 0.0, 0.0)
			Bi_2 (0.5, 0.0, 0.0)
			Bi_3 (0.0, 0.5, 0.0)
$B_xGa_{1-x}As$	0.062	B (0.0, 0.0, 0.0)	–
	0.125	B_1 (0.5, 0.0, 0.0)	–
		B_2 (0.0, 0.5, 0.0)	
	0.187	B_1 (0.0, 0.0, 0.0)	–
		B_2 (0.5, 0.0, 0.0)	
		B_3 (0.0, 0.5, 0.0)	
$B_xGa_{1-x}As_{1-y}Bi_y$	(0.062, 0.062)	B (0.00205, 0.99959, 0.99795)	Bi (0.62904, 0.87671, 0.73971)
	(0.062, 0.125)	B (0.00373, 0.99851, 0.00944)	Bi_1 (0.62944, 0.36989, 0.75214)
			Bi_2 (0.62882, 0.87510, 0.73917)
	(0.062, 0.187)	B (0.99386, 0.00924, 0.01815)	Bi_1 (0.62935, 0.36972, 0.75418)
			Bi_2 (0.11370, 0.88910, 0.78224)
			Bi_3 (0.62848, 0.87636, 0.74015)
	(0.125, 0.062)	B_1 (0.00126, 0.99975, 0.99727)	Bi (0.63029, 0.87082, 0.74071)
		B_2 (0.00095, 0.49890, 0.99890)	
	(0.125, 0.125)	B_1 (0.99477, 0.00152, 0.00954)	Bi_1 (0.62240, 0.33870, 0.75836)
		B_2 (0.49042, 0.12454, 0.00158)	Bi_2 (0.62779, 0.85491, 0.73211)
	(0.125, 0.187)	B_1 (0.99360, 0.00910, 0.01718)	Bi_1 (0.62842, 0.36932, 0.74141)
		B_2 (0.49113, 0.24330, 0.01345)	Bi_2 (0.11622, 0.89067, 0.77610)
			Bi_3 (0.61335, 0.89103, 0.76907)
	(0.187, 0.062)	B_1 (0.00270, 0.99982, 0.99824)	Bi (0.61662, 0.88393, 0.77092)
		B_2 (0.49036, 0.00991, 0.01628)	
		B_3 (0.00146, 0.49838, 0.00141)	
	(0.187, 0.125)	B_1 (0.00349, 0.99902, 0.99807)	Bi_1 (0.63016, 0.36996, 0.73786)
		B_2 (0.49077, 0.00581, 0.01314)	Bi_2 (0.61697, 0.88367, 0.76821)
		B_3 (0.00393, 0.49883, 0.99832)	
	(0.187, 0.187)	B_1 (0.99420, 0.00917, 0.01621)	Bi_1 (0.63049, 0.37018, 0.73677)
		B_2 (0.49150, 0.00746, 0.01082)	Bi_2 (0.11363, 0.88530, 0.76722)
		B_3 (0.00358, 0.49616, 0.99393)	Bi_3 (0.61619, 0.88363, 0.77523)

Table 2
Calculated lattice constant *a*(Å) and bulk modulus *B*(GPa) of zinc blende GaAs, BAs, GaBi, and BBi compounds using the GGA-WC functional, compared to previous theoretical results and available experimental data.

Binary	Lattice constant (Å)			Bulk modulus (GPa)		
	Present work	Previous results	Experiment results	Present work	Previous results	Experiment results
GaAs	5.668	5.75[a]–5.57[b]	5.65[c]	68.656	61.78[a]–81.92[b]	77[d]
BAs	4.777	4.81[e]–4.76[f]	4.77[g]	139.28	132.4[e]–150.23[f]	–
GaBi	6.327	6.30[h]–6.30[i]	6.32[c]	42.372	43.65[h]–43.25[i]	–
BBi	5.470	5.46[j]–5.52[k]	–	76.544	81.89[j]–72. 209[k]	–

[a] Ref. [27].
[b] Ref. [28].
[c] Ref. [29].
[d] Ref. [30].
[e] Ref. [31].
[f] Ref. [32].
[g] Ref. [33].
[h] Ref. [18].
[i] Ref. [17].
[j] Ref. [34].
[k] Ref. [35].

Fig. 3 shows the variation of the lattice constant of $GaAs_{1-x}Bi_x$ alloys as a function of Bi concentration for the relaxed and unrelaxed structure, using the GGA-WC and GGA-PBE approximations for the concentration x range $0 \leq x \leq 1$.

It is clearly seen that the lattice constant of the relaxed $GaAs_{1-x}Bi_x$ alloys varied linearly with concentration x (perfectly obey to the Vegard's law), with a bowing parameter equal to −0.02114 and −0.00834 Å for the GGA-WC and GGA-PBE approximations, respectively. Our results of bowings are much smaller than the ones reported by other authors, D. Madouri et al. [37] of $b = -0.38$ Å for the relaxed alloys and Reshak et al. [27] of $b = -1.00$ Å for unrelaxed ones, using GGA-PBE approximation, for concentration x range up to 1.

Table 3
Calculated lattice constant a(Å) and bulk modulus B(GPa) for $GaAs_{1-x}Bi_x$, $B_xGa_{1-x}As$ and $B_xGa_{1-x}As_{1-y}Bi_y$ alloys. The lattice mismatch ($\Delta a/a$) is calculated between the alloys and the GaAs substrate.

Alloys	Concentrations	Lattice constant (Å)			Bulk modulus (GPa)			Mismatch (%)
		Present work	Theoretical results	Experiment results	Present work	Theoretical results	Experiment results	Present work
$GaAs_{1-x}Bi_x$	0.062	5.701	–	–	64.343	–	–	0.582
	0.125	5.742	–	–	62.738	–	–	1.305
	0.187	5.786	–	–	60.262	–	–	2.081
$B_xGa_{1-x}As$	0.062	5.606	–	–	70.600	–	–	1.093
	0.125	5.550	–	–	73.534	–	–	2.081
	0.187	5.497	–	–	76.752	–	–	3.016
$B_xGa_{1-x}As_{1-y}Bi_y$	(0.062, 0.062)	5.665	5.76[a]	–	68.696	–	–	0.052
	(0.062, 0.125)	5.705	–	–	73.004	–	–	0.652
	(0.062, 0.187)	5.747	–	–	66.084	–	–	1.393
	(0.125, 0.062)	5.612	5.71[a]	–	70.257	–	–	0.988
	(0.125, 0.125)	5.669	5.76[a]	–	76.870	–	–	0.017
	(0.125, 0.187)	5.694	–	–	70.087	–	–	0.458
	(0.187, 0.062)	5.552	5.66[a]	–	72.009	–	–	2.046
	(0.187, 0.125)	5.594	5.72[a]	–	80.869	–	–	1.305
	(0.187, 0.187)	5.634	–	–	75.470	–	–	0.599

[a] Ref. [16].

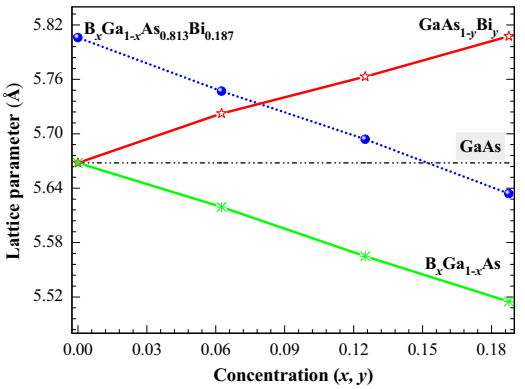

Fig. 2. Lattice constant as a function of B and Bi concentrations in $B_xGa_{1-x}As_{1-y}Bi_y$ alloys, for x and $y \leq 0.187$.

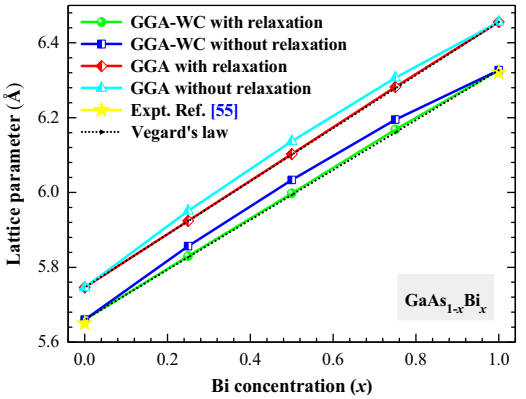

Fig. 3. Lattice parameter as a function of Bi concentration in $GaAs_{1-x}Bi_x$ alloys for the relaxed and unrelaxed structure, with x range $0 \leq x \leq 1$.

For $B_xGa_{1-x}As_{1-y}Bi_y$ alloys, the lattice parameter decreases fairly linearly with increasing of B amount, with bowing parameter of about −0.064 Å. This leads to minimize the mismatch between $B_xGa_{1-x}As_{1-y}Bi_y$ alloys and GaAs substrate, from 2.081% (for B = 0) to 0.559% (for B = 0.187), susceptible to reduce the strain effect and epitaxial layers defects.

$B_{0.125}Ga_{0.875}As_{0.875}Bi_{0.125}$ is expected to be lattice matched to GaAs substrate, with a mismatch less than 0.017%, witch is useful to design QWs with high structural quality.

Table 4
Calculated direct (Γ-Γ) and indirect (Γ-X) band gaps (eV) of zinc blende GaAs, BAs, GaBi and BBi compared with available experiment and theoretical data.

Binary		Present work			Theoretical results	Experiment results
		GGA-PBE	GGA-WC	TB-mBJ		
GaAs	$E_{\Gamma-\Gamma}$	0.479	0.355	1.492	0.33[a]–1.56[b]	1.52[c]
	$E_{\Gamma-X}$	1.483	1.348	2.128	1.51[d]	1.98[e]
BAs	$E_{\Gamma-\Gamma}$	3.277	3.256	3.707	3.46[f]–3.34[g]	–
	$E_{\Gamma-X}$	1.438	1.348	1.870	1.20 [h]	–
GaBi	$E_{\Gamma-\Gamma}$	0.000	0.000	−0.148	0.23 [i]–−1.38[j]	−1.45[c]
	$E_{\Gamma-X}$	0.870	0.788	1.403	1.10[i]	–
BBi	$E_{\Gamma-\Gamma}$	0.356	0.347	0.632	0.61[k]	–
	$E_{\Gamma-X}$	0.876	0.793	1.254	–	

[a] Ref. [38].
[b] Ref. [39].
[c] Ref. [40].
[d] Ref. [31].
[e] Ref. [41].
[f] Ref. [42].
[g] Ref. [43].
[h] Ref. [44].
[i] Ref. [11].
[j] Ref. [27].
[k] Ref. [29].

3.2. Electronic properties

3.2.1. Band structure

A Binary parent compounds

First, the electronic band structure of zinc blende binary GaAs, BAs, GaBi and BBi compounds are computed based on self-consistent scalar relativistic FP-LAPW calculations in which the exchange-correlation potential was treated by the TB-mBJ in addition with GGA-PBE and GGA-WC functionals.

The calculated band gaps of GaAs, BAs, GaBi and BBi are listed in Table 4, and the present results are well compared with available experimental data and other theoretical values.

The zinc blende GaAs, GaBi and BBi have direct-band gaps of 1.492, −0.148 and 0.632 eV, respectively, while BAs has an indirect-band gap of 1.870 eV according to the TB-mBJ potential.

The band gaps obtained from TB-mBJ exchange potential are found to be in excellent agreement with experimental data. But, GGA-PBE and GGA-WC functionals are underestimated the band gaps. This is due to the limitation of GGA within DFT theory [45].

B Ternary and quaternary $B_xGa_{1-x}As_{1-y}Bi_y$ alloys

Second, the electronic band structure of zinc blende ternary $GaAs_{1-x}Bi_x$, $B_xGa_{1-x}As$ and quaternary $B_xGa_{1-x}As_{1-y}Bi_y$ alloys are studied for different compositions (x, y) (0.062, 0.125 and 0.187), using FP-LAPW method within the TB-mBJ exchange potential and GGA-PBE scheme.

The band structures for $GaAs_{0.812}Bi_{0.187}$, $B_{0.187}Ga_{0.812}As$ and $B_{0.187}Ga_{0.812}As_{0.812}Bi_{0.187}$ alloys are plotted in Fig. 4 along the various symmetry lines of Brillouin zone (BZ).

It is clearly seen that the valence band maximum (VBM) and conduction band minimum (CBM) occurs at the Γ symmetry point of the Brillouin zone for all alloys. Thus, the zinc blende $GaAs_{1-x}Bi_x$, $B_xGa_{1-x}As$ and $B_xGa_{1-x}As_{1-y}Bi_y$ alloys have direct band gap energy, favors the optical transitions which is of great interest for emission and absorption in optoelectronic devices.

The calculated band gaps for zinc blende $GaAs_{1-x}Bi_x$, $B_xGa_{1-x}As$ and $B_xGa_{1-x}As_{1-y}Bi_y$ alloys are listed in Table 5.

Fig. 5 shows the variation of direct (Γ-Γ) and indirect (Γ-X) band gaps for $GaAs_{1-x}Bi_x$ as a function of concentration x (range up to 0.187), using the TB-mBJ and GGA-PBE approaches.

The direct band gap (Γ-Γ) decreases with increasing Bi content in GaAs (∼308 meV per x = 0.187), while it increases slightly with increasing B content (∼73 meV per x = 0.187). A large derivation from Vegard's law is obtained for relaxed $GaAs_{1-x}Bi_x$ alloys, with b = 2.16 eV, according to the mBJ approach, for x up to 0.187. This strong value is due to significant differences in atomic size and electronegativity between Bi and As atoms in $GaAs_{1-x}Bi_x$ alloys.

Our result of the direct band gap bowing is close to those obtained by Janotti et al. [14] of b = 2.1 eV using LDA approach with small Bi composition and Madouri et al. [37] of b = 1.74 eV using the GGA approach, for the composition range $0 < x < 1$.

Fig. 6 shows the variation of direct (Γ-Γ) and indirect (Γ-X) band gaps as a function of B for different Bi concentrations in $B_xGa_{1-x}As_{1-y}Bi_y$ alloys using TB-mBJ exchange potential. It is clearly seen that the direct band gap increases non-linearly with B content.

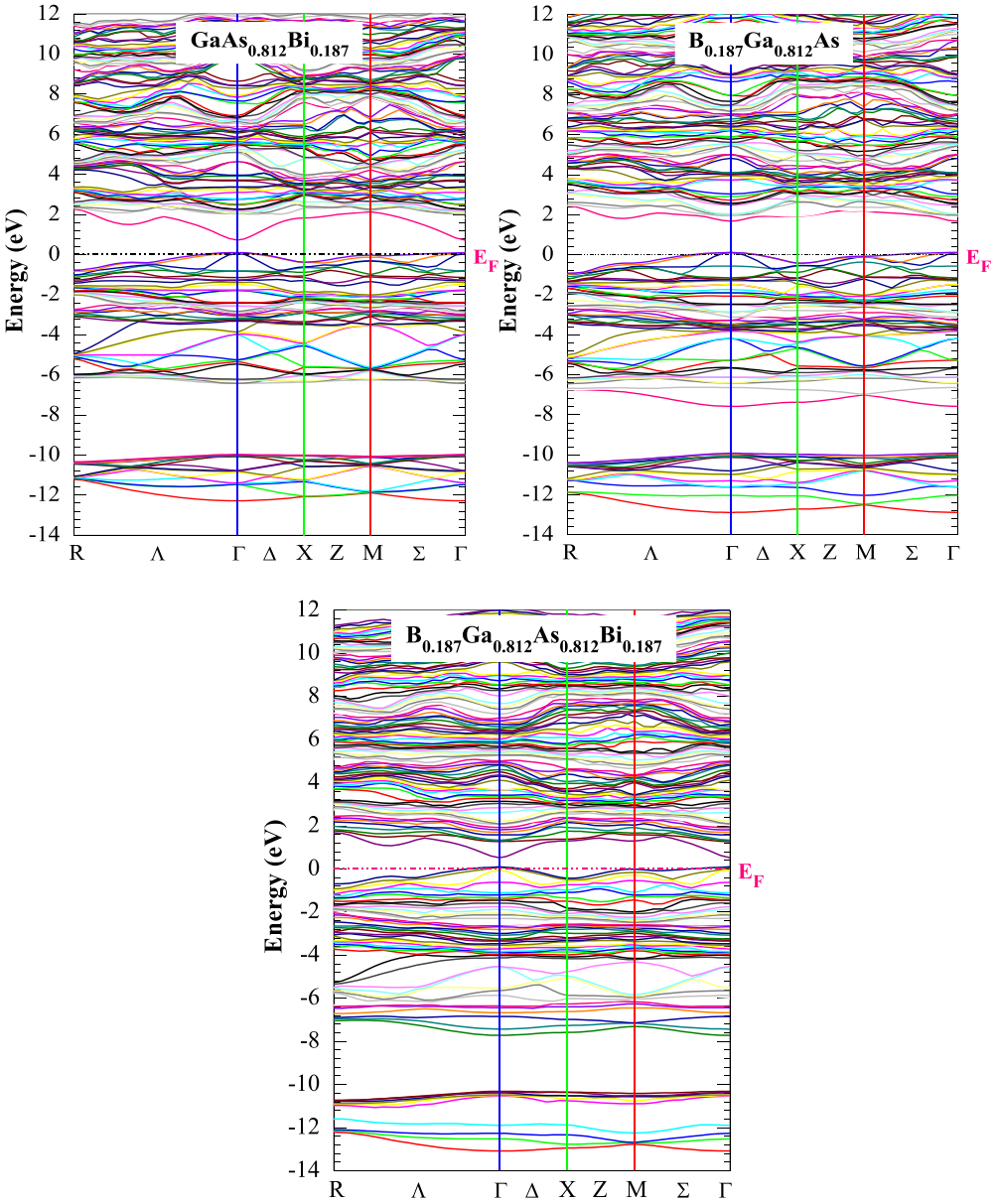

Fig. 4. Band structures for $GaAs_{0.812}Bi_{0.187}$, $B_{0.187}Ga_{0.812}As$ and $B_{0.187}Ga_{0.812}As_{0.812}Bi_{0.187}$ alloys calculated using TB-mBJ potential. The Fermi level is set to zero.

A $B_xGa_{1-x}As_{1-y}Bi_y$ alloy with concentrations ($x = 0.125$, $y = 0.125$) has a small direct band gap of about 0.938 eV corresponds to the optical wavelength 1.32 μm, near to the optical fiber communication wavelength (~1.3 μm).

Thus, $B_xGa_{1-x}As_{1-y}Bi_y$ lattice-matching to GaAs is very useful for the design of high-efficiency infrared QW Laser, which could an alternative to GaNAsBi/GaAs Laser Diode realized by M. Yoshimoto et al. [46].

3.2.2. *Density of states*

Fig. 7 shows the total density of states (TDOS) and partial (PDOS) of $B_xGa_{1-x}As_{1-y}Bi_y$ alloys, calculated using mBJ exchange potential for ($x = 0.187$, $y = 0.187$).

The total DOS can be divided into three regions, two located in the valence band called (VB_{low}, VB_{higher}) below the Fermi level (E_F) and the conduction band (CB) region above the Fermi level. The lowest region (VB_{low}) located in the energy range from −13 to −10 eV is mainly dominated by the As-5*s* and Bi-6*s* states. While, the highest region (VB_{higher}) below the Fermi level is divided into two sub-bands. The first one extends from −7.5 to −4 eV formed essentially by B-*s* and Ga-4*s* states, with small contribution from As-5*p* and Bi-6*p* states. The second region near the top of valence band is formed by hybridization

Table 5
Calculated direct (Γ-Γ) and indirect (Γ-X) band gaps (eV) of zinc blende $GaAs_{1-x}Bi_x$, $B_xGa_{1-x}As$ and $B_xGa_{1-x}As_{1-y}Bi_y$ alloys.

Alloys			Present work			
	Concentrations		GGA-PBE	TB-mBJ	Theoretical results	Experiment results
$GaAs_{1-x}Bi_x$	0.062	E_{Γ_Γ}	0.146	1.148	–	–
		E_{Γ_X}	1.381	1.971	–	–
	0.125	E_{Γ_Γ} E_{Γ_X}	0.039	0.899	–	–
			1.278	1.835	–	–
	0.187	E_{Γ_Γ} E_{Γ_X}	0.007	0.635	–	–
			1.176	1.720	–	–
$B_xGa_{1-x}As$	0.062	E_{Γ_Γ} E_{Γ_X}	0.495	1.509	–	–
			1.391	1.971	–	–
	0.125	E_{Γ_Γ} E_{Γ_X}	0.593	1.522	–	–
			1.311	1.881	–	–
	0.187	E_{Γ_Γ} E_{Γ_X}	0.705	1.565	–	–
			1.245	1.818	–	–
$B_xGa_{1-y}As_{1-x}Bi_y$	(0.062, 0.062)	E_{Γ_Γ} E_{Γ_X}	0.244	1.178	–	–
			1.237	1.773	–	–
	(0.062, 0.125)	E_{Γ_Γ} E_{Γ_X}	0.038	0.924	–	–
			1.106	1.623	–	–
	(0.062, 0.187)	E_{Γ_Γ} E_{Γ_X}	0.040	0.683	–	–
			1.088	1.526	–	–
	(0.125, 0.062)	E_{Γ_Γ} E_{Γ_X}	0.322	1.209	–	–
			1.003	1.678	–	–
	(0.125, 0.125)	E_{Γ_Γ} E_{Γ_X}	0.013	0.938	–	–
			1.555	1.507	–	–
	(0.125, 0.187)	E_{Γ_Γ} E_{Γ_X}	0.064	0.689	–	–
			1.110	1.387	–	–
	(0.187, 0.062)	E_{Γ_Γ} E_{Γ_X}	0.456	1.267	–	–
			1.100	1.604	–	–
	(0.187, 0.125)	E_{Γ_Γ} E_{Γ_X}	0.185	0.946	–	–
			0.951	1.431	–	–
	(0.187, 0.187)	E_{Γ_Γ} E_{Γ_X}	0.016	0.705	–	–
			0.883	1.284	–	–

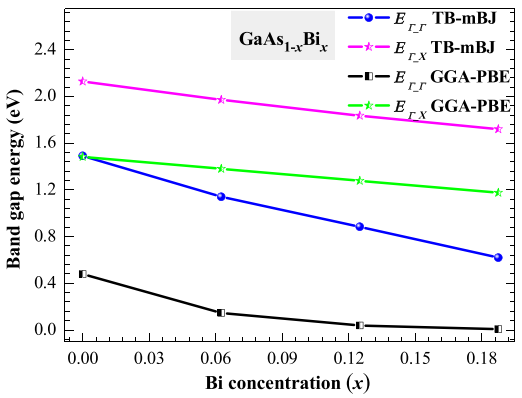

Fig. 5. Direct (Γ-Γ) and indirect (Γ-X) band gap energies as a function of concentration x for $GaAs_{1-x}Bi_x$ calculated using GGA-PBE and TB-mBJ approaches.

between B-2p, Ga-4p, As-5p and Bi-6p states. The conduction band (CB) region is mainly dominated by B-2p state, with small contribution from Ga-4p, As-5p and Bi-6p states.

As it can be seen in Fig. 7, the valence band maximum (VBM) and the conduction band minimum (CBM) are mainly contributed by Bi-6p and B-2p states, respectively. Thus, the large reduction of $B_xGa_{1-x}As_{1-y}Bi_y$ band gap when induced of Bi content is due to resonant interaction between the valence band maximum VBM and 6p state of Bi atom, consistent with previous reports [14,47]. While the resonance interaction between 2p state of B-induced and the conduction band minimum CBM causes a slight increase of the band gap.

3.3. Optical properties

The optical properties of $B_xGa_{1-x}As_{1-y}Bi_y$ alloys are investigated using FP-LAPW method based on the modified Becke-Johnson (TB-mBJ) potential, with varying B and Bi concentrations up to 0.187.

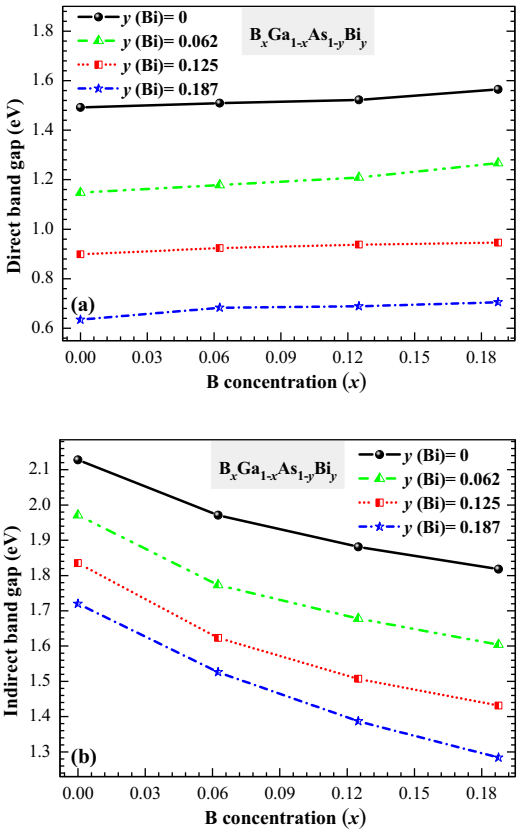

Fig. 6. Direct (Γ-Γ) (a), indirect (Γ-X) (b) band gaps as a function of B and Bi concentrations in $B_xGa_{1-x}As_{1-y}Bi_y$ alloys calculated using TB-mBJ potential.

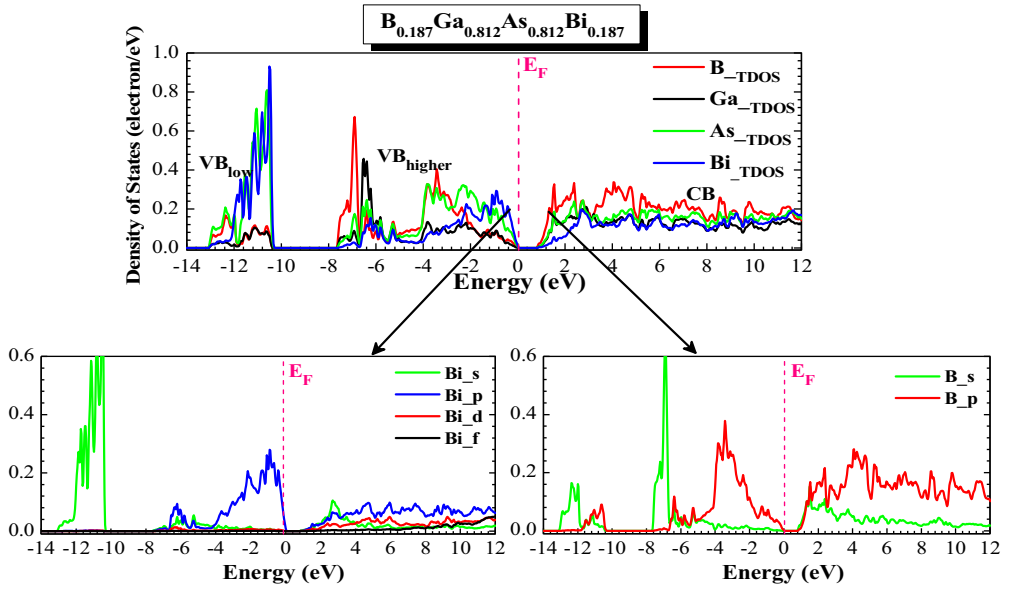

Fig. 7. Total (TDOS) and partial (PDOS) density of $B_xGa_{1-x}As_{1-y}Bi_y$ alloys calculated using TB-mBJ potential, for x and $y = 0.187$.

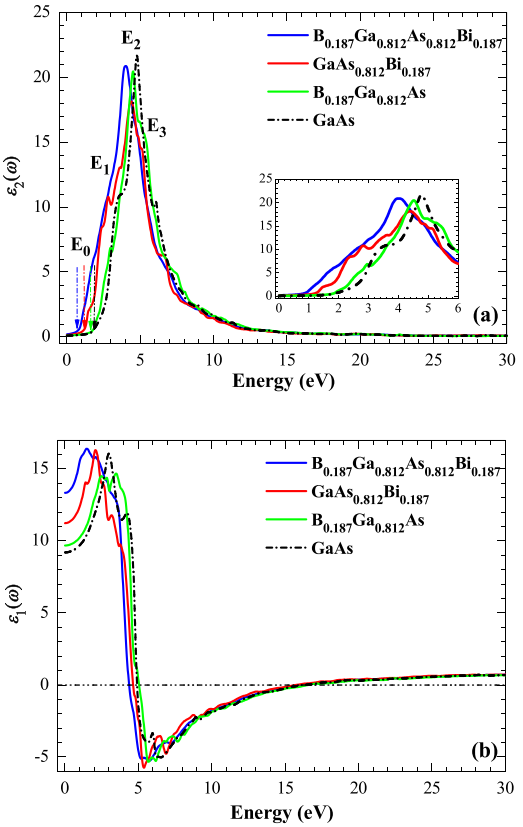

Fig. 8. The calculated (a) imaginary part $\varepsilon_2(\omega)$ and (b) real part $\varepsilon_1(\omega)$ of the dielectric function for $B_xGa_{1-x}As_{1-y}Bi_y$ alloys using TB-mBJ potential.

The optical constants can be deduced from the complex dielectric function $\varepsilon(\omega)$:

$$\varepsilon(\omega) = \varepsilon_1(\omega) + i\varepsilon_2(\omega) \tag{2}$$

where: $\varepsilon_1(\omega)$ and $\varepsilon_2(\omega)$ are the real and imaginary parts of the dielectric function, respectively.

The imaginary part of the dielectric function, $\varepsilon_2(\omega)$ is calculated directly from the momentum matrix elements between the occupied and the unoccupied eigenstates. The relation between the real part $\varepsilon_1(\omega)$ and imaginary part $\varepsilon_2(\omega)$ of the dielectric function is given by the Kramers-Kronig relation [48]. The knowledge of both the real and the imaginary parts of the dielectric function allows the calculation of important optical functions.

The optical constants such as refractive index $n(\omega)$, reflectivity $R(\omega)$ and absorption coefficient $\alpha(\omega)$ can be calculated from the flowing relations [49,50]:

$$n(\omega) = \frac{\left[\varepsilon_1^2(\omega) + \varepsilon_2^2(\omega)\right]^{\frac{1}{2}} + \varepsilon_1(\omega)}{2} \tag{3}$$

$$R(\omega) = \frac{[n-1]^2 + k^2}{[n+1]^2 + k^2} \tag{4}$$

$$\alpha(\omega) = \frac{4\pi}{\lambda} k(\omega) \tag{5}$$

where: k is the extinction coefficient; λ is the wave length of light in the vacuum.

The calculated real and imaginary parts of the dielectric function for $B_xGa_{1-x}As_{1-y}Bi_y$ alloys for the photon energy range up to 30 eV are displayed in Fig. 8.

The curves of $\varepsilon_2(\omega)$ in Fig. 8 (a) indicate that the absorption edges of the dielectric function occurs at 2.11, 1.81, 1.15 and 0.82 eV for GaAs, $B_{0.187}Ga_{0.812}As$, $GaAs_{0.812}Bi_{0.187}$ and $B_{0.187}Ga_{0.812}As_{0.812}Bi_{0.187}$, respectively. These critical points represent the threshold for the direct optical transitions from the VBM to the CBM at Γ_{15v}–Γ_{1c} symmetry. Beyond the absorption edges, the spectra of $\varepsilon_2(\omega)$ exhibit three intense peaks 'E_1', 'E_2' and 'E_3' correspond to the interband transitions. For $B_xGa_{1-x}As_{1-y}Bi_y$ alloys, the most optical transitions contribute to these peaks occur from the occupied B-2*p*, Ga-4*p*, As-5*p* and Bi-6*p* states localized in highest valence band to the unoccupied B-2*p*, Ga-4*p*, As-5*p* and Bi-6*p* states localized in lowest conduction band

Table 6
Calculated peak positions of $\varepsilon_2(\omega)$ (in eV) and static optical constants $\varepsilon_1(0)$, $n(0)$ and $R(0)$ for GaAs, $B_{0.187}Ga_{0.812}As$, $GaAs_{0.812}Bi_{0.187}$, and $B_{0.187}Ga_{0.812}As_{0.812}Bi_{0.187}$ compounds.

	Peak positions (in eV)				Static optical constants		
Components	E_0	E_1	E_2	E_3	$\varepsilon_1(0)$	$n(0)$	$R(0)$ (%)
GaAs	2.11	3.48	4.77	6.08	9.20–13.20[a]–13.43[b]	3.03–3.64[a]–3.66[b]	25.43
$B_{0.187}Ga_{0.812}As$	1.81	2.94	4.52	5.48	9.68	3.11	26.38
$GaAs_{0.812}Bi_{0.187}$	1.15	2.82	4.38	5.15	11.23	3.35	29.21
$B_{0.187}Ga_{0.812}As_{0.812}Bi_{0.187}$	0.82	2.56	4.02	5.02	13.33	3.65	32.50

[a] Ref. [51].
[b] Ref. [52].

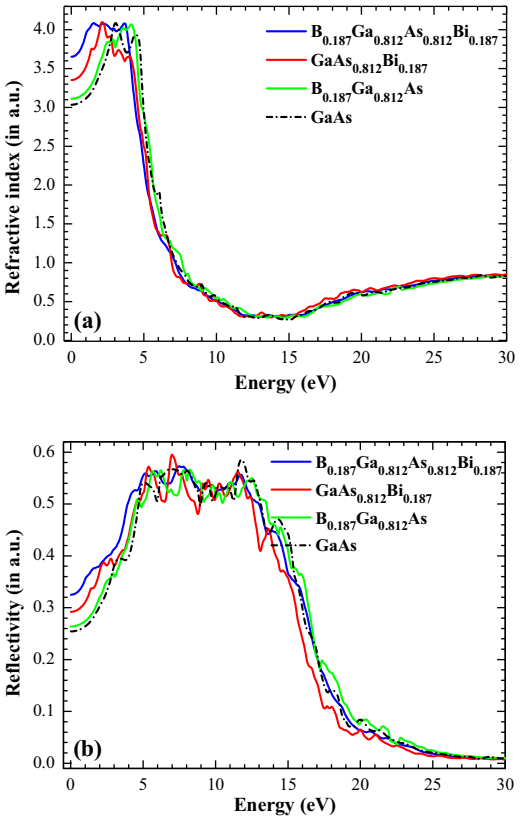

Fig. 9. Refractive index $n(\omega)$ (a) and reflectivity $R(\omega)$ (b) for $B_xGa_{1-x}As_{1-y}Bi_y$ alloys calculated using TB-mBJ potential.

along R, Γ and X symmetry direction in the Brillouin Zone. We observe that the peaks position shifts towards lower energies and significant increases in their amplitude occur with increasing the B and Bi contents.

In Table 6, we summarize the peak positions, static dielectric constant $\varepsilon_1(0)$, static refraction index $n(0)$ and static reflectivity $R(0)$ for GaAs, $B_{0.187}Ga_{0.812}As$, $GaAs_{0.812}Bi_{0.187}$ and $B_{0.187}Ga_{0.812}As_{0.812}Bi_{0.187}$ compounds.

It is clearly seen in Fig. 8 (b) that the static dielectric constant increases with increasing both B and Bi amounts from 9.20 (for x and $y = 0$) to 13.33 (for x and $y = 0.187$). But, Bi-induced affects more the static dielectric constant than B-induced.

Fig. 9 (a) and (b) shows the spectra of refractive index $n(\omega)$ and reflectivity $R(\omega)$ for $B_xGa_{1-x}As_{1-y}Bi_y$ alloys. The incorporation of B and Bi amounts in $B_xGa_{1-x}As_{1-y}Bi_y$ alloys significantly increase the static refractive index with 62% from 3.03 (for x and $y = 0$) to 3.65 (for x and $y = 0.187$). This step in refractive index (Fig. 9 (a)) between $B_{0.187}Ga_{0.812}As_{0.812}Bi_{0.187}$ and GaAs confine the light, which is interesting to be used as an active layer in high-efficiency QW Lasers.

Furthermore, the maximum refractive index is reached in the photon energy range of [0.70−4.80] eV, which increases with B and Bi contents. The main peak for BGaAsBi is related mainly to the 'E_2' transition of 3.96 eV.

It can be seen from Fig. 9 (b), that the maximum reflectivity occurs in the photon energy range of [3.40–14.60] eV. The maximum reflectivity is related to the resonance plasmon appearing in the ultraviolet region. For higher energy ($E > 15$ eV), the reflectivity decreases quickly.

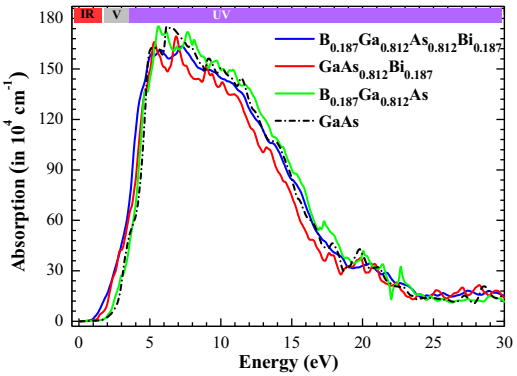

Fig. 10. Absorption coefficient $\alpha(\omega)$ for $B_xGa_{1-x}As_{1-y}Bi_y$ alloys calculated using TB-mBJ potential.

The absorption in semiconductors occurs when the photon energy of the incident beam is higher than E_g ($h\nu > E_g$) causes excitation of the ground state electrons from the VB to the CB.

The calculated absorption coefficient $\alpha(\omega)$ for $B_xGa_{1-x}As_{1-y}Bi_y$ alloys is plotted in Fig. 10. At low energies, beyond the absorption adges, the curves show a fast increasing absorption, which decrease at higher energies (at around 12.0 eV). The maximum absorption occurs in the photon energy range of [3.50–14.70] eV, corresponding to ultraviolet region. Furthermore, the incorporation of B and Bi slightly reduces the maximum value of absorption.

4. Conclusion

To summarize, we have performed FP-LAPW calculation to study the structural, electronic and optical properties of the dilute boron-bismide semiconductor $B_xGa_{1-x}As_{1-y}Bi_y$ alloys matched to GaAs. The computed structural parameters using GGA-WC are found to be in good agreement with experimental data. Bismide semiconductors $GaAs_{1-x}Bi_x$ and $B_xGa_{1-x}As_{1-y}Bi_y$ alloys obey Vegard law when the lattice relaxation is taking into account. While the band gap gives strong bowing parameters due to significant differences in atomic size and electronegativity between constituent atoms alloys. The band structure and density of states of these compounds are well predicted by Tran–Blaha-modified Becke–Johnson (TB-mBJ). $B_xGa_{1-x}As_{1-y}Bi_y$ alloy is expected to be lattice matched to GaAs substrate for ($x = 0.125$, $y = 0.125$) with a mismatch less than 0.017%, witch is useful to design QWs with high interface quality. The B and Bi induced into GaAs allows to the reduction of the band gap energy. The effect of B and Bi contents on the optical properties of $B_xGa_{1-x}As_{1-y}Bi_y$ alloys was investigated. The static optical constants increase with increasing B and Bi contents. $B_xGa_{1-x}As_{1-y}Bi_y$ alloys show strong absorption in energy range of [3.50–14.70] eV, corresponding to the UV region, which is of great importance for designing high-efficiency solar cells.

$B_xGa_{1-x}As_{1-y}Bi_y$ lattice-matching to GaAs with band gap cover the optical fiber communication wave band is very useful as an active layer/barrier in single quantum wells (SQW) for the design of advanced infrared QW optoelectronic devices as Laser Diodes.

Acknowledgments

The author A. Assali thanks Dr. Anderson Janotti (University of Delaware, USA) for precious help. The author A.H. Reshak would like to acknowledge the CENTEM project, reg. no. CZ.1.05/2.1.00/03.0088, cofunded by the ERDF as part of the Ministry of Education, Youth and Sports OP RDI programme and, in the follow-up sustainability stage, supported through CENTEM PLUS (LO1402) by financial means from the Ministry of Education, Youth and Sports under the National Sustainability Programme I. Computational resources were provided by MetaCentrum (LM2010005) and CERIT-SC (CZ.1.05/3.2.00/08.0144) infrastructures.

References

[1] S. Francoeur, M.J. Seong, A. Mascarenhas, S. Tixier, M. Adamcyk, T. Tiedje, Appl. Phys. Let. 82 (2003) 3874.
[2] Y. Zhang, A. Mascarenhas, L.-W. Wang, Phys. Rev. B 71 (2005) 155201.
[3] B. Fluegel, S. Francoeur, A. Mascarenhas, S. Tixier, E.C. Young, T. Tiedje, Phys. Rev. Lett. 97 (2006) 067205.
[4] T. Tiedje, E.C. Young, A. Mascarenhas, Int. J. Nanotechnol. 5 (2008) 963–983.
[5] R.B. Lewis, D.A. Beaton, X. Lu, T. Tiedje, J. Cryst. Growth 311 (2009) 1872–1875.
[6] N. Hossain, I.P. Marko, S.R. Jin, K. Hild, S.J. Sweeney, R.B. Lewis, D.A. Beaton, T. Tiedje, Appl. Phys. Lett. 100 (2012) 051105.
[7] J. Yoshida, T. Kita, O. Wada, K. Oe, Jpn. J. Appl. Phys. 42 (2003) 371.
[8] K. Oe, H. Okamato, Jpn. J. Appl. Phys. 37 (1998) 1283–1285.
[9] E.C. Young, M.B. Whitwick, T. Tiedje, D.A. Beaton, Phys. Status Solidi C 5 (2007) 1707–1710.
[10] H. Achour, S. Louhibi, B. Amrani, A. Tebboune, N. Sekkal, Superlattices Microstruct. 44 (2008) 223–229.
[11] A. Abdiche, H. Abid, R. Riane, A. Bouaza, Phys. B 405 (2010) 2311–2316.

[12] A.H. Reshak, H. Kamarudin, S. Auluck, J. Alloys Compd. 509 (2011) 9685–9691.
[13] Y. Zhang, M.J. Kappers, D. Zhu, F. Oehler, F. Gaob, C.J. Humphreys, Sol. Energy Mater. Sol. Cells 117 (2013) 279–284.
[14] A. Janotti, Su-Huai Wei, S.B. Zhang, Phys. Rev. B 65 (2002) 115203.
[15] D.A. Beaton, A.J. Ptak, K. Alberi, A. Mascarenhas, J. Cryst. Growth 351 (2012) 37–40.
[16] (a) B.G. Aslana, M. Yalcin, Eur. Phys. J. B 88 (2015) 312;
(b) W. Kohn, L.J. Sham, Phys. Rev. A 140 (1965) 1133.
[17] P. Hohenberg, W. Kohn, Phys. Rev. B 136 (1964) 864.
[18] F.P. Blaha, K. Schwarz, G.K.H. Madsen, D. Kvasnicka, J. Luitz, WIEN2k: an augmented plane wave + Local orbitals program for calculating crystal properties, wien, Austria, karlheinz schwarz, Techn. Univ. (2011) (ISBN: 3-950131-1-2).
[19] Z. Wu, R.E. Cohen, Phys. Rev. B 73 (2006) 235116.
[20] F. Tran, P. Blaha, Phys. Rev. Lett. 102 (2009) 226401.
[21] J.P. Perdew, K. Burke, M. Ernzerhof, Phys. Rev. Lett. 77 (1996).
[22] H.J. Monkhorst, J.D. Pack, Phys. Rev. 13 (1976) 5188.
[23] F.D. Murnaghan, Proc. Natl. Aced. Sci. U. S. A. 30 (1944) 244–247.
[24] M.I. Ziane, Z. Bensaad, T. Ouahrani, B. Labdelli, H. Ben Nacer, H. Abid, Mater. Sci. Semicond. Process. 16 (2013) 1138–1147.
[25] Z. Charifi, H. Baaziz, F. El Haj Hassan, N. Bouarissa, J. Phys. Condens. Matter (2005) 174083.
[26] P. Dufek, P. Blaha, K. Schwarz, Phys. Rev. B 50 (1994) 7279.
[27] A.H. Reshak, H. Kamarudin, S. Auluck, I.V. Kityk, J. Solid State Chem. 186 (2012) 47–53.
[28] F. Benkabou, Z. Chelahi Chikr, H. Aourag, Pierre J. Becker, Phys. Lett. A 252 (1999) 71.
[29] S. Cui, W. Feng, H. Hua, Z. Feng, Y. Wang, Comput. Mater. Sci 47 (2010) 968–972.
[30] M. Ferhat, A. Zaoui, Phys. Rev. B 73 (2006) 115107.
[31] M. Guemou, B. Bouhafs, A. Abdiche, R. Khenata, Y. Al Douri, S. Bin Omran, Phys. B 407 (2012) 1292–1300.
[32] Numerical data and functional relationships in science and technology, in: O. Madelung, M. Schulz (Eds.), Landolt-Bornstein, New Series, Group III, vol. 22, Springer-Verlag, Berlin, 1987 (pt.a).
[33] S. Azzi, A. Zaoui, M. Ferhat, Solid State Commun. 144 (2007) 245–248.
[34] O. Madelung (Ed.), Semiconductors-Basic Data, Springer-Verlag, New York, 1996.
[35] K.H. Hellwege, O. Madelung, Landolt-Bornstein, Semiconductors Physics of Group IV Elements and III–V Alloys, New Series, Group III (1982).
[36] G. Mendoza-Diaz, K. Stevens, A. Schwartzman, R. Beresford, J. Cryst. Growth 178 (1997) 45–55.
[37] D. Madouri, A. Boukra, A. Zaoui, M. Ferhat, Comput. Mater. Sci 43 (2008) 818–822.
[38] F. El Haj Hassan, A.V. Postnikov, O. Pagès, J. Alloys Compd. 504 (2010) 559–565.
[39] M.I. Ziane, Z. Bensaad, T. Ouahrani, H. Bennacer, Mater. Sci. Semicond. Process. 30 (2015) 181–196.
[40] Numerical data and functional relationships in science and technology, in: O. Madelung, M. Schulz (Eds.), Landolt-Bornstein, New Series, Group III, vol. 22, Springer-Verlag, Berlin, 1987 (pt.a).
[41] M. Briki, M. Abdelouhab, A. Zaoui, M. Ferhat, Superlattices Microstruct. 45 (2009) 80–90.
[42] D. Merabet, R. Rached, S. Khenata, B. Benalia, N. Abidri, S. Bettahar, Phys. B 406 (2011) 3247–3255.
[43] N. Chimot, J. Even, H. Folliot, S. Loualiche, Phys. B 364 (2005) 263.
[44] H. Meradji, S. Labidi, S. Ghemid, S. Drablia, B. Bouhafs, Phys. Proc. 2 (2009) 933–940.
[45] Y. Kawazoe, Bull. Mater. Sci. 26 (2003) 13–17.
[46] M. Yoshimoto, W. Huang, G. Feng, Y. Tanaka, K. Oe, J. Cryst. Growth 301–302 (2007) 975–978.
[47] Y. Zhang, A. Mascarenhas, L.-W. Wang, Phys. Rev. B 71 (2005) 155201.
[48] P.Y. Yu, M. Cardona, Fundamentals of Semiconductors: Physics and Materials Properties, Springer-Verlag, Berlin, 1999, p. 233.
[49] C.A. Draxl, R. Abt, The Calculation of Optical Properties Within WIEN97, ICTP lecture notes, un published, 1998.
[50] Y. Zhang, A. Mascarenhas, L.-W. Wang, Phys. Rev. B 71 (2005) 155201.
[51] S. Adachi, Optical Constants of Crystalline and Amorphous Semiconductors, Kluwer Academic, Boston, 1999.
[52] D.E. Aspnes, A.A. Studna, Dielectric functions and optical parameters of Si, Ge, GaP, GaAs, GaSb, InP, InAs, and InSb from 1.5 to 6.0 eV, Phys. Rev. B 27 (1983) 985.